Morphodynamic adaptation of a tidal basin to centennial sea-level rise
The importance of lateral expansion

Guo, Leicheng; Xu, Fan; van der Wegen, Mick; Townend, Ian; Wang, Zheng Bing; He, Qing

DOI
10.1016/j.csr.2021.104494

Publication date
2021

Document Version
Final published version

Published in
Continental Shelf Research

Continental Shelf Research 226 (2021) 104494

Contents lists available at ScienceDirect

Continental Shelf Research

journal homepage: www.elsevier.com/locate/csr

Morphodynamic adaptation of a tidal basin to centennial sea-level rise: The importance of lateral expansion

Leicheng Guo [a,*], Fan Xu [a], Mick van der Wegen [b,c], Ian Townend [d], Zheng Bing Wang [a,c,e], Qing He [a]

[a] State Key Lab of Estuarine and Coastal Research, East China Normal University, Shanghai 200241, China
[b] IHE Delft, Delft, the Netherlands
[c] Deltares, Delft, the Netherlands
[d] School of Ocean and Earth Sciences, University of Southampton, Southampton, UK
[e] Faculty of Civil Engineering and Geosciences, Delft University of Technology, Delft, the Netherlands

ARTICLE INFO

Keywords:
Tidal basin
Sea-level rise
Accommodation space
Morphodynamic modeling

ABSTRACT

Global climate changes have accelerated sea-level rise (SLR), which exacerbates the risks of coastal flooding and erosion. It is of practical interest to understand the long-term hydro-morphodynamic adaptation of coastal systems to SLR at a century time scale. In this work we use a numerical model to explore morphodynamic evolution of a schematized tidal basin in response to SLR of 0.25–2.0 m over 100 years with special emphasis on the impact of lateral basin expansion. Starting from a sloped initial bed, morphodynamic development of the system leads to the formation of alternating bars and meandering channels inside the tidal basin and an ebb-tidal delta extending seaward from the basin. Imposing rising sea level causes progressive inundation of the low-lying floodplains, found along the basin margins, inducing an increase in basin plain area and tidal prism, as well as intertidal area and storage volume. Although the overall channel-shoal structure persists under SLR, lateral shoreline expansion alters the basin hypsometry, leading to enhanced sediment export. The newly-submerged floodplains partly erode, supplying sediment to the system for spatial redistribution, hence buffering the impact of SLR. The vertical accretion rate of the tidal flats inside the tidal basin lags behind the rate of SLR. However, lateral shoreline migration under SLR creates new intertidal flats, compensating intertidal flat loss in the original basin. In contrast, a constrained tidal basin without low-lying floodplains is subject to profound drowning and tidal flat losses under SLR. Overall, the model results suggest that an unconstrained tidal system allowing lateral shoreline migration has buffering capacity for alleviating the drowning impact of SLR by evolving new intertidal areas, sediment redistribution and morphodynamic adjustment. These findings suggest that preserving tidal flats located along the margins of tidal basins (instead of reclaiming them) sustains the system's resilience to SLR.

1. Introduction

Coastal areas and wetlands provide important habitats for human beings and ecosystems (Craft et al., 2009; Muis et al., 2016). However, rising sea levels are posing a threat to populated or protected areas, leading to coastal erosion, shoreline retreat, loss of salt-marshes, and increasing risk of flooding (Nicholls et al., 1999). The global mean sea-level rise (SLR) rate has been estimated at 1.8 ± 0.1 mm yr^{-1} between 1880 and 1980 (Douglas, 1991), increasing to 3.4 ± 0.4 mm yr^{-1} over the interval 1993–2014 (Nerem et al., 2010; Chen et al., 2017). Although local SLR rates vary slightly in different studies (Dangendorf et al., 2017; Frederikse et al., 2020), it is generally accepted that the rate of SLR is globally accelerating and will continue to accelerate in the future (IPCC, 2014; Chen et al., 2017). It has become a worldwide concern that tidal flat accretion in estuaries and coasts may not be able to keep pace with an accelerated rate of SLR in the coming century. This results in submergence and loss of tidal flats and salt-marshes and associated important habitats and ecosystems (Craft et al., 2009; Kirwan and Megonigal, 2013; Valiela et al., 2018), such as in the Wadden Sea (van Wijnen and Bakker, 2001; Wang et al., 2018; Lodder et al., 2019),

* Corresponding author.
E-mail address: lcguo@sklec.ecnu.edu.cn (L. Guo).

https://doi.org/10.1016/j.csr.2021.104494
Received 17 September 2020; Received in revised form 9 June 2021; Accepted 7 July 2021
Available online 10 July 2021

San Francisco Bay (Takekawa et al., 2013), and the Mississippi River delta (Blum and Roberts, 2009). Global estimates suggest that 40–90% of coastal wetlands may be lost by the end of the 21st century even when considering marsh accretion and expansion (Ganju et al., 2017; Valiela et al., 2018). The decline in river-borne sediment supply and land subsidence may further accelerate the coastal wetland loss (Syvitski et al., 2009).

There is an ongoing debate about the likely impact of an accelerating rate of SLR on estuaries and deltas in the forthcoming century, which is the period of most relevance for present coastal management and planning. In river-dominated deltas, SLR causes delta submergence, shoreline recession and changes in habitat depending on the availability of fluvial sediment and the rate of SLR (van de Lageweg and Slangen, 2017). Differing from open coasts and river deltas, the impact of SLR on tidal basins and estuaries tends to be more complicated because of the non-linear behavior of tidal wave propagation, the interactions between basin geometry and tidal flats, and large-scale estuarine morphodynamic adjustment and feedback mechanism in response to SLR (Du et al., 2018; Lodder et al., 2019). Furthermore, whilst marine transgression on the open coast is invariably normal to the shoreline, the changes in an estuary are more 3-dimensional. For clarity, we consider changes along the axis (thalweg) of the estuary to take place landward, for example, if the tidal limit extends further inland. In contrast, lateral changes are those that are normal to the axis or cross-shore, such as erosion of the shoreline which causes a lateral expansion of the estuary.

Many previous studies have documented changes in tidal wave propagation and hydrodynamics when imposing a higher mean sea level on a fixed morphology (Friedrichs et al., 1990; Wolanski and Chappell, 1996; Du et al., 2018; Talke and Jay, 2020). These studies have stressed the importance of tidal basin planform variations under different water levels and consequent impacts on tidal wave propagation and sediment transport. Others have examined the large-scale response of flats and channels using aggregated models (van Goor et al., 2013; Townend et al., 2016). Examining the likely response, whilst taking account of the redistribution of sediments and the potential changes in morphology, has received far less attention. Schuerch et al. (2018) estimated that 0–30% of the global coastal wetland might be lost until 2100 provided that sediment supply remains at present levels and that there were no constraints on shoreline migration. This estimated loss is smaller than previous predictions, because of the assumed possible inland expansion, where new wetlands are created. Ladd et al. (2019) and Mariotti and Carr (2014) also stressed that sediment from the lateral erosion of tidal flats might provide sources for vertical accretion. These studies emphasize how tidal systems are able to adjust their own morphology as part of the dynamic response to SLR. They imply that the fate of a tidal system to be drowned or not, depends on its ability to accrete vertically at rates equal to or larger than SLR, and/or to migrate inland at rates faster than shoreline erosion. However, the mechanisms and modes of morphological adjustment that would enable tidal basins to adapt to SLR at the decade to century time scales, when considering both vertical accretion and horizontal migration, are not yet clear. The main evidence for possible mechanisms relies on studies of shoreline retreat and system transgression from sedimentary stratigraphic studies over historic and geological time scales (Allen, 1990; Townend and Pethick, 2002; Dalrymple et al., 2006).

Large-scale morphodynamic modeling is a powerful tool in exploring the impact of SLR on estuarine and coastal morphodynamics at the decade to century time scales. Modeling approaches range from highly schematized box-models (e.g., Rossington et al., 2007) to case studies including complex process interactions (e.g., van der Wegen, 2013). Based on an aggregated approach considering morphological equilibrium concepts (van Goor et al., 2003; Wang et al., 2018; Lodder et al., 2019), it was suggested that a tidal inlet-basin system, like those in the Dutch Wadden Sea, can survive SLR up to a rate of 15 mm yr^{-1} owing to the sediment import from ebb-tidal deltas. In contrast, process-based models take complex process descriptions as a starting point. This type of model has a high spatial and temporal resolution but is computationally more expensive than an aggregated approach. The morphodynamic modeling approach has been applied to schematized tidal lagoons and estuaries (Dissanayake et al., 2012; van Maanen et al., 2013; van der Wegen, 2013) and also to actual estuaries and tidal basins, such as the sub-embayments of San Francisco Bay (Ganju and Schoellhamer, 2010; Elmilady et al., 2019; Zhang et al., 2020) and the Western Scheldt Estuary (Dam et al., 2013). Most of the past studies documented that intertidal flats in tidal lagoons and estuaries are prone to drown under an accelerating rate of SLR (van der Wegen, 2013; van der Wegen et al., 2016; van de Lageweg and Slangen, 2017; Elmilady et al., 2019).

The above-mentioned modeling studies highlight the morphodynamic sensitivity to SLR rates and the high probability of drowning of tidal basins under enhanced rates of SLR scenarios. An important yet under-explored aspect of estuarine adaptation to SLR is the presence of lateral migration of the estuary shoreline, leading to an expansion of plan area under rising sea levels and its subsequent impact on tidal dynamics and morphodynamic evolution. Many tidal basins and estuaries worldwide have a convergent planform and are fringed by large areas of low-lying lands in the lower reaches, which are currently just above high water (see Fig. 1 and S1 in the Supporting Information; Dalrymple and Choi, 2007; Bamunawala et al., 2020). Moreover, the low relief of coastal plain tidal basins and estuaries implies that a relatively small increase in mean sea level can lead to a large increase in intertidal area (Kirby, 2000; Friedrichs, 2011). This will have an impact on tidal propagation, subtidal flow and salinity distribution, sediment transport and associated morphodynamic adaptations. Lateral expansion under SLR potentially allows the survival of intertidal flats and marsh systems. Sustainable coastal management strategies, e.g., by introducing more flexible flood protection schemes, could be better developed if there is more knowledge on the benefit of preserving low-lying lands. Therefore, it would be of substantial value for coastal management to understand the degree to which large-scale estuarine morphodynamics adapt to SLR of different rates.

The objective of this work is to explore the morphodynamic impact of SLR on a long tidal basin at the centennial time scale when considering the possibility of lateral expansion by using a process-based numerical modeling approach. We first outline the modeling method and settings before presenting the model results in terms of morphological evolution, tidal dynamics and net sediment transport. We then assess the impact of SLR and the implications for estuary management.

2. Method

We construct a 2D model of a schematized tidal basin based on the Delft3D software (Lesser et al., 2004) which is a process-based model widely used in modeling estuarine and coastal morphodynamics (see e.g., van der Wegen, 2013; Guo et al., 2015). The model domain is 250 km long and 100 km wide. Longitudinally, the first 150 km is prescribed as a long tidal basin which meets an open coastal ocean extending 100 km offshore (Fig. 2a). The tidal basin width at the mean sea level increases from 1 km at the landward end ($x = 0$) to 15 km at the mouth section ($x = 150$ km), with an initially funnel-shaped planform (Fig. 2a). The width convergence length is approximately 270 km (Table 1). The model mesh has a high resolution of 50 m cell size along the tidal basin and around the mouth regions to resolve the channels and shoals formed therein, while the cell size increases slowly to 200 m towards the seaward boundary where morphodynamic changes remain limited. The main channel of the tidal basin has a linearly sloping bed from 0 m at the landward end to 15 m at the mouth section, and further deepens to 50 m at the seaward boundary 100 km offshore (Fig. 2b). The initial cross-section profile combines a U-shape in the more landward reach ($x = 0$ to $x = 50$ km, Fig. 2c) and a concave inter- and supra-tidal flat profile in the seaward reach ($x = 50$ km to $x = 150$ km, Fig. 2d). The transverse inter-tidal flat slope is 1/500–1/1500 on average in the lower basin, which is close to the mean value observed in actual estuaries (Le Hir

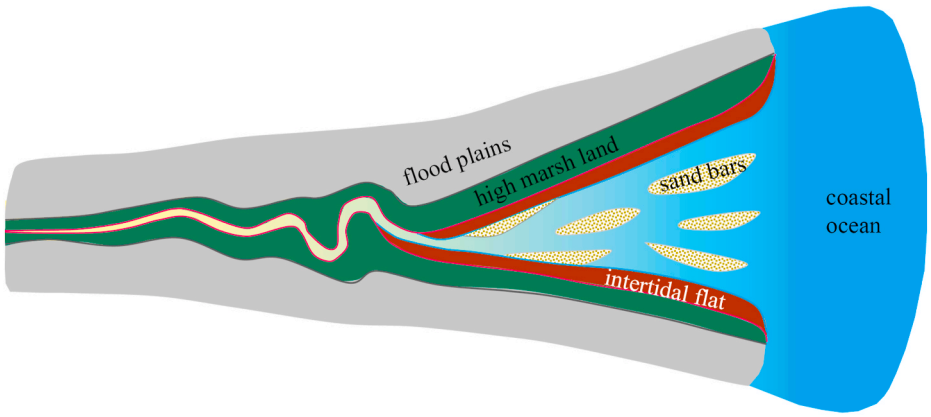

Fig. 1. A conceptual diagram of a tide-dominated estuary with mid-channel sand bars, flanked tidal flats and marsh land, and low-lying floodplains, modified from Dalrymple and Choi (2007).

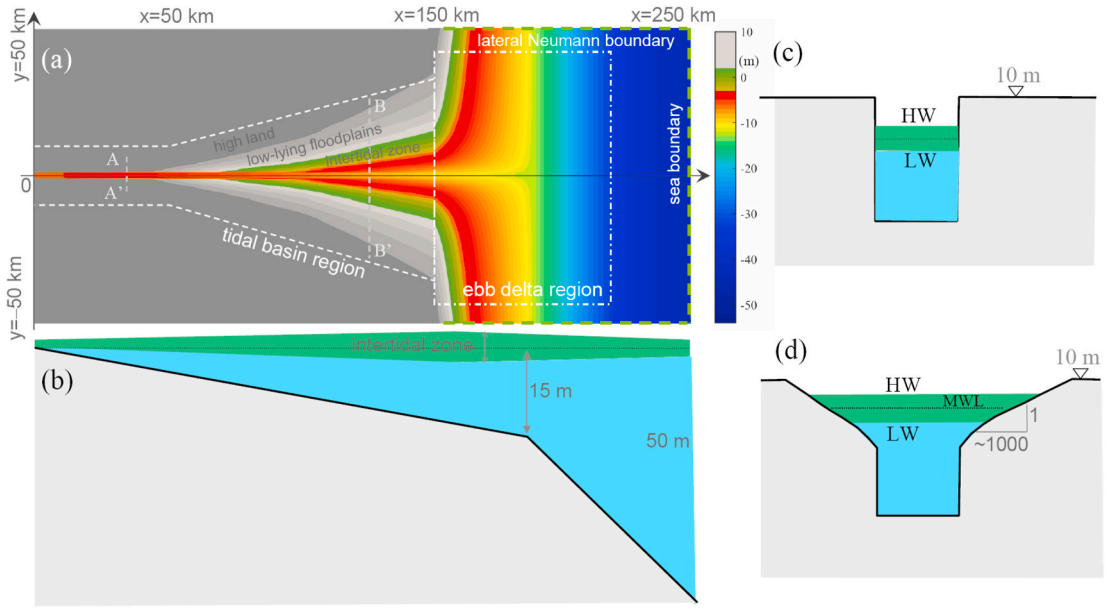

Fig. 2. Sketches of the schematized model domain setting in distorted space scales: (a) the planform of the tidal basin with division between the inner basin and the outer delta regions, (b) a side view of the main channel and initial bed profile, and (c, d) cross-section profiles of A-A′ and B–B′, respectively. The green shading indicates the inter-tidal zone. Both the bank and the bed are erodible. The dashed and dash-dotted boxes in panel (a) indicate the regions of tidal basin and the ebb-tidal delta, respectively. (For interpretation of the references to colour in this figure legend, the reader is referred to the Web version of this article.)

Table 1
Model parameter settings based on the Delft3D software.

Property	Parameter
domain size	(150 + 100) km*100 km
cell size	50–200 m
initial channel bed slope	1/10000
width convergence	convergence length L_b of 270 km (using $B=B_o e^{-Lb/x}$)
lateral flat slope	1/500–1/1500
bed roughness	uniform Chézy 65 $m^{1/2}/s$
horizontal eddy viscosity	1 m^2/s
tidal amplitude	1.5 m at the seaward boundary
sediment	sand of 150 μm in median size
sediment transport formula	Engelund and Hansen (1967)
hydrodynamic time step	60 s
hydrodynamic run time	5 years + 1 year
morphological factor	100
morphodynamic time	500 years + 100 years
dry bed erosion parameter	100%
lateral bed slope factor (alfaBn)	10

et al., 2000). The concave tidal flat shape is chosen to be consistent with the fact that tidal flats are more broadly present in the highly convergent regions of tidal basins and estuaries close to the coasts (Dalrymple and Choi, 2007) and that tidal flats under tidal forcing controls and with minor wave influence are more likely to develop concave profiles (Kirby, 2000; Friedrichs, 2011).

The tidal basin is driven by tides with no river flow and fluvial sediment supply and excludes wave impact and density difference effects. For reasons of simplicity, an astronomical semi-diurnal M_2 tide with amplitude of 1.5 m is imposed at the seaward boundary. Other tidal constituents such as S_2 and M_4 are not considered although including them would increase tidal range and high-water level, which may induce more inundation. It is assumed that the tides at the seaward boundary will not change much under SLR. Tidal propagation into the tidal basin does, however, adapt in response to morphological changes. The two lateral boundaries of the sea domain are prescribed as Neumann boundary conditions, following Roelvink and Walstra (2004), with no water level gradient in the direction normal to the lateral boundaries. The high land of the tidal basin domain (the dark shade region in Fig. 2a)

has an elevation of 10 m (above mean sea level) and is not inundated even at high tide, hence free-slip boundaries are imposed there. A uniform friction of Chézy coefficient 65 $m^{1/2}/s$ is used. Sediment transport is prescribed by one single sand fraction (a median grain size of 150 μm) treated as total load transport by the Engelund and Hansen (1967) formula. Morphodynamic development is accelerated by using a morphological factor approach based on the Exner equation (Roelvink and Reniers, 2011). Similar to Guo et al. (2015), a morphological factor of 100 is used to accelerate bed level update in this work.

To enable channel migration and dry land erosion, the function of dry bed erosion is activated. Dry and wet cells are classified by a depth threshold of 0.1 m (Deltares, 2011). In addition, the dry cells adjacent to a wet cell are assumed to be erodible and the erosion volume of the dry cell is prescribed by a user-defined fraction (0–100%) of the erosion in the wet cell. Previous modeling studies considering dry cell erosion show that a fraction of 100% is suitable to reproduce sand bar erosion and channel migration (van der Wegen and Roelvink, 2008; Guo et al., 2015), and is used in this study as well. Moreover, bed slope effects on the sediment transport are considered using the Ikeda (1982) and Bagnold (1966) methods, with longitudinal and lateral bed slope adjustment factors of 5 and 10, respectively (Table 1). The secondary flow impact is considered, whereas the Coriolis effect, land subsidence and uplift, and vegetation controls are not considered at this moment.

For this study, we first run a morphodynamic simulation for 500 years during which channels and shoals take shape inside the tidal basin and sediment deposition at the mouth builds up an ebb-tidal delta. The morphology at the end of 500 years (see Fig. 4a) is then used as the initial condition for sensitivity simulations considering SLR. We continue the morphodynamic simulation for another 100 years without SLR, as a reference scenario. It is projected that the most likely SLR by 2100 is some 0.44 m (ranging from 0.26 to 0.61 m), 0.53 m (0.36–0.71 m), and 0.74 m (0.52–0.98 m) according to the Representative Concentration Pathway (RCP) scenarios 2.6, 4.5 and 8.5, respectively, while a high-end scenario suggests a rise of 2–2.5 m (Church et al., 2013). Accordingly, in this study four sensitivity scenarios are defined by imposing SLR of 0.25, 0.5, 1.0, and 2.0 m over 100 years as an exponential increase (Fig. 3), which equates to mean SLR rates of 2.5, 5, 10, and 20 mm yr^{-1}, respectively. To assist comparison of the situation without lateral expansion, we also ran extra simulations by imposing thin dams along the high water shorelines, as defined by the model results at the end of the initial 500-year simulation. This has the effect of removing the low-lying floodplains, with elevations above the high water, from the model domain, so that they are not flooded in the following 100-year simulations even under SLR, representing a diked and constrained tidal basin in which lateral expansion is not allowed (see section 4.1). Selected morphodynamic properties are compared with the reference scenario to highlight the impact of SLR, including the erosion and deposition pattern, the variations of inter-tidal flat area and storage volume, and tidal wave dynamics and tidally-averaged sediment transport.

3. Model results

3.1. Morphodynamic evolution

The initial 500-year morphodynamic simulation leads to the development of meandering channels and shoal systems inside the tidal basin and the formation of an ebb-tidal delta with bifurcating channels seaward of the basin mouth. Given no external sediment sources, erosion of the channel bed and channel banks inside the tidal basin and spatial redistribution of the sediment initiates the morphodynamic changes. The ebb-tidal delta builds up rapidly by sediment export from the basin that leads to continuous delta progradation. The morphodynamic development gradually slows down after 500 years when a matured channel-shoal structure takes shape and the change rates decline (see supplementary animation A1). However, it is noteworthy that a static morphodynamic equilibrium might have not been reached, according to the classification of Zhou et al. (2017).

The morphology at the end of 500 morphodynamic years is then used as the initial bathymetry of the 100-year simulations considering SLR (see supplementary animation A2). Although the overall channel-shoal pattern is sustained in the SLR scenarios (Fig. 4a–e), channel migration and sand bar movement continue inside the tidal basin, leading to strong erosion and deposition (Fig. 4f–i). Under rising sea-level conditions, the shoreline within the tidal basin laterally migrates across the low-lying land (Figs. 5 and S3), and the lateral expansion is more significant under higher SLR. For instance, the maximum lateral migration distance is up to 5 km in the SLR 2.0 scenario. Other than the adjustment of channels and shoals in the SLR scenarios, the newly-submerged floodplains undergo slight erosion (Fig. 5). On the seaward side, the ebb-tidal delta continues to grow over the 100 years in all scenarios (see Fig. S2). The ebb-tidal delta progradation, however, is smaller in magnitude in the SLR scenarios compared with the reference case, as indicated by the seaward extent of the ebb-tidal delta shoreline (Fig. 4f–i). Higher SLR causes more land inundation in the tidal basin and less progradation of the ebb-tidal delta.

The plan area and bankfull width (at high water) of the tidal basin increases with rising sea-levels (see Fig. S3). As lateral expansion is more significant in the seaward part of the tidal basin owing to the prescribed tidal flat profile, the width convergence rate becomes slightly larger

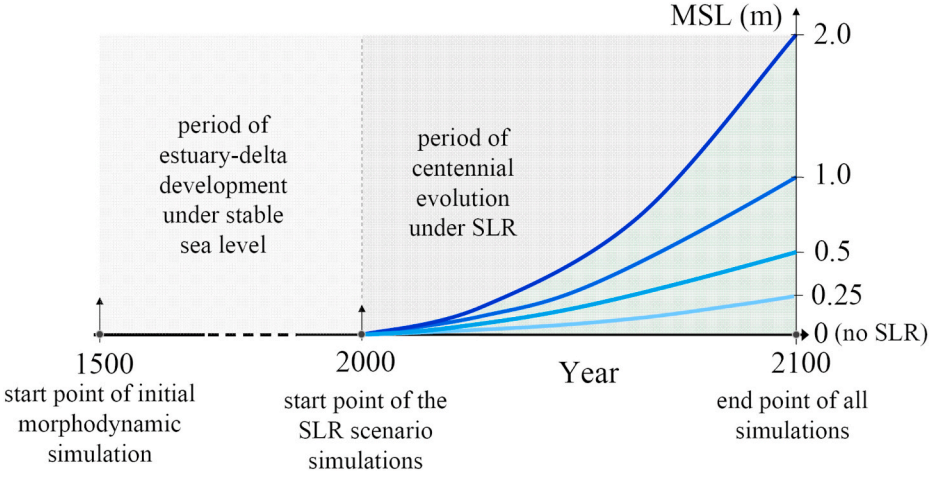

Fig. 3. A sketch showing mean sea level changes in the morphodynamic time framework considering different rates of SLR. The first 500 years are squeezed in time scale as indicated by the dashed line.

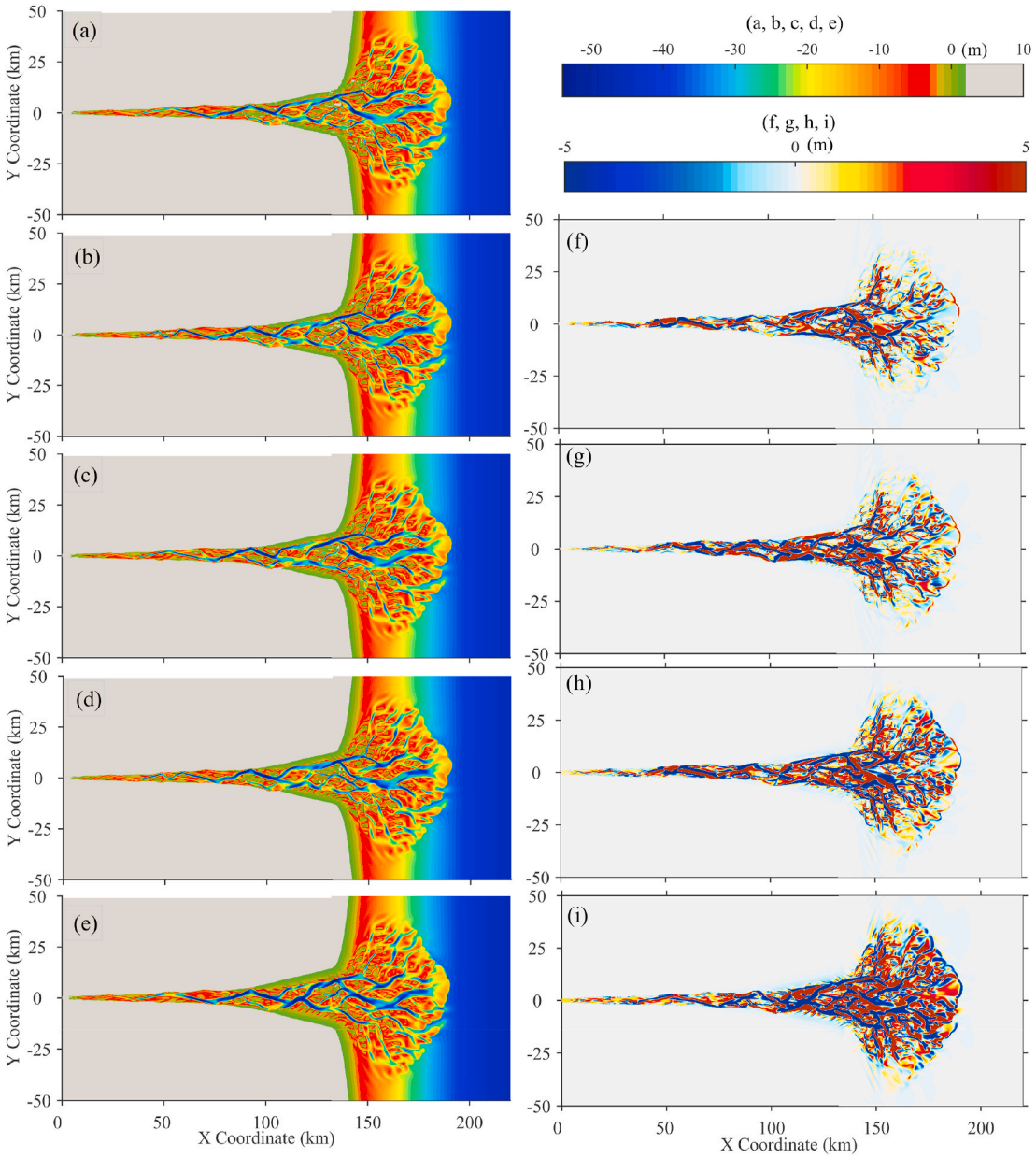

Fig. 4. The morphology after 100 years considering (a) no SLR, SLR of (b) 0.25 m, (c) 0.5 m, (d) 1.0 m, and (e) 2.0 m, and accordingly bathymetry differences between the reference scenario and the scenarios with SLR of (f) 0.25 m, (g) 0.5 m, (h) 1.0 m, and (i) 2.0 m. The green shading in panels (a) to (e) roughly indicates inter-tidal zone. The dashed lines in panels (f) to (i) indicate the 2 m elevation contour in the reference scenario and the solid lines are the 2 m elevation contour in the SLR scenarios. Positive values in panels (f) to (i) indicate accretion while negative values indicate erosion in the SLR scenarios compared to the reference case. The bed elevation in panels (b) to (e) is referenced to the raised mean sea levels in the SLR scenarios, with the elevation of MSL raised by 0.25 m, 0.5 m, 1.0 m and 2.0 m, respectively. (For interpretation of the references to colour in this figure legend, the reader is referred to the Web version of this article.)

under SLR (Fig. S3). Moreover, the cross-sectionally averaged bed levels largely increase in elevation with SLR (see Fig. S4), owing to larger lateral expansion and accretion on the shoals than offsetting the extent of channel deepening. However, the cross-sectionally averaged water depth, which was calculated as the ratio of cross-sectional area to cross-sectional width at the surface, may decrease in the SLR scenarios, because there is a greater increase in cross-sectional width than in cross-sectional area.

3.2. Tidal dynamics and net sediment export

At the beginning of the 100-year sensitivity simulations, the amplitudes of the tides traveling into the tidal basin are amplified because the effect of width convergence is stronger than frictional damping. The tidal amplitude increases slowly from 1.5 m at the seaward boundary to 2 m at the basin mouth, and further to 3.8 m inside the estuary before reducing to zero at the landward boundary (see Fig. S5). In addition, significant overtides like M_4 (up to 0.75 m in amplitude) are generated internally. The tidal wave deformation exhibits longer falling tide than rising tide, and the peak ebb currents are stronger than the flood currents (see Fig. S6), suggesting overall ebb dominance of sand transport within the tidal basin. The stronger peak ebb currents are ascribed to the combined impact of a seaward residual current induced by Stokes return flow and the hydraulic storage effect of the intertidal flats which is likely to enhance ebb currents. The former results in a seaward mean water gradient, with the mean water level elevated by up to 0.5 m at the landward end (see Fig. S4), and predominantly seaward residual currents (see Fig. S7).

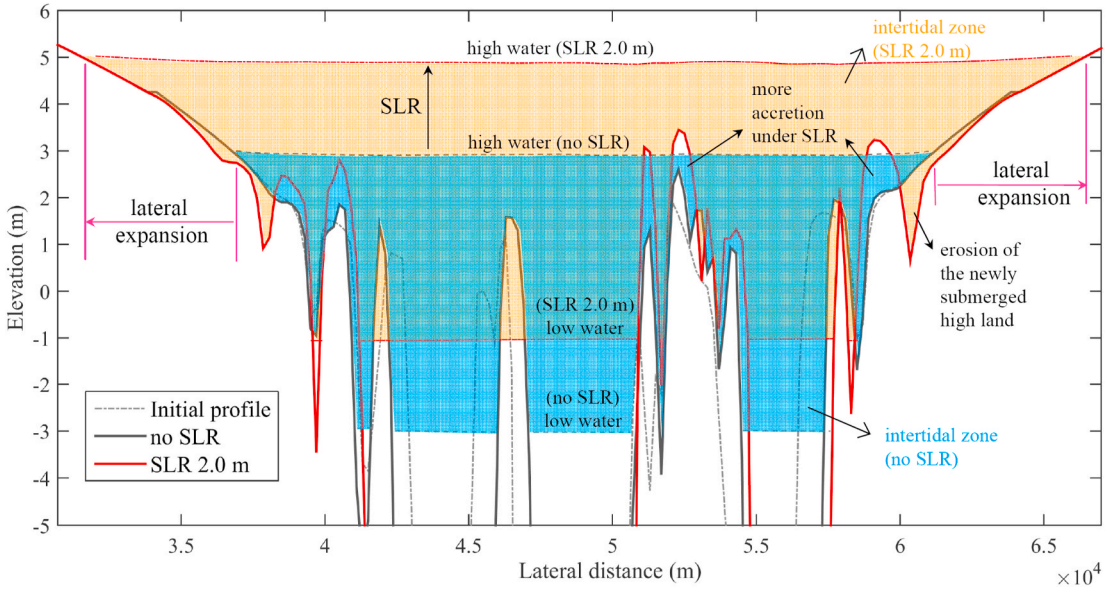

Fig. 5. Changes of a cross-section profile at x = 130 km (the deeper part of the channel segment is not shown) and associated high water and low water changes in the reference run and 2.0 m SLR scenario including lateral expansion and extra erosion of the newly-submerged inland zone under SLR.

The amplitudes of the tides are slightly more amplified by the end of the 100-year simulation for the reference scenario because of the deepening of the main channel (Fig. S5). This also holds true for all other scenarios, while the tides in the 2.0 m SLR scenario are slightly more amplified compared with the reference case. Changes in the internally generated M_4 tide are small under SLR. Overall, the changes in tidal range caused by SLR are insignificant in this study. However, as the surface plan area and cross-section area increase with rising sea levels, the tidal prism of the tidal basin increases with SLR, e.g., by up to 27% in the 2.0 m SLR scenario compared with the reference case (see Fig. S9). This increase in tidal prism is mainly ascribed to larger surface area under higher mean sea levels, rather than any increase in tidal range.

The tidal changes lead to sediment transport adjustment. In the reference scenario, the net sediment transport flux at the mouth section of the tidal basin, i.e., the interface between the inner basin and outer delta at x = 150 km, is persistently seaward (see Fig. 2a), indicating continuous sediment export from the tidal basin towards the outer ebb-tidal delta (Fig. 6a). This is in line with the ebb dominance already noted. Other than the landward net sediment transport in the utmost upstream regions (which explains the accretion and shoaling therein), the tidally-averaged sediment transport remains predominantly seaward while its magnitude increases in the seaward direction (see Fig. S8). Moreover, SLR enhances the seaward sediment export rate and a higher SLR leads to more sediment export (Fig. 6a). The impact of SLR on the sediment export from the constrained basin remains very limited (Fig. 6b). The impact of SLR is not significant in the first 50 years and is more pronounced when the mean sea level becomes higher. Specifically, the cumulated sediment export over 100 years is approximately 25% larger under a SLR of 2.0 m compared with the reference scenario (Fig. 6a).

3.3. Tidal flat evolution

In order to check whether the intertidal flats would survive SLR, we calculate the intertidal flat area based on the integrated areas of the cells with elevation between high water and low water envelopes. To reveal the effect of vertical accretion of the previously present tidal flats and the effect of lateral expansion under SLR, two types of intertidal flat areas are calculated: (1) using a fixed frame for all bathymetries over the 100 years, with the initial high and low water envelopes as the fixed

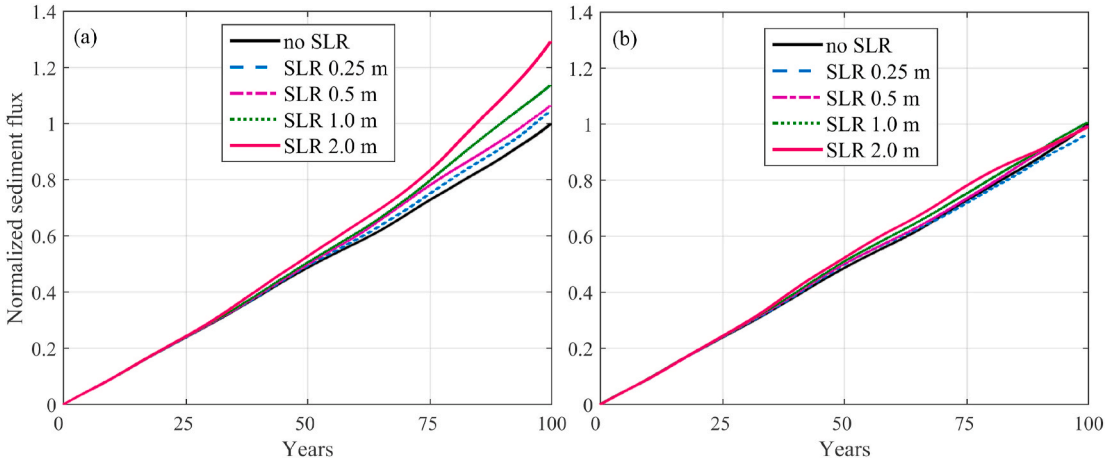

Fig. 6. The cumulative sediment flux at the mouth section over the 100 years which are normalized by the cumulated flux in the no SLR scenario: (a) unconstrained tidal basin with low-lying lands, and (b) constrained tidal basin in which expansion to low-lying land is not allowed.

frame of reference and computing the intertidal area between the two surfaces, and (2) using a moving frame over the 100 years, with gradually adapted high and low water envelopes in response to SLR as a moving frame of reference to compute the intertidal area (see Fig. S10). Changes in the former intertidal areas mainly reflect the net accretion or erosion of the initially present tidal flats, while the latter indicates the combined effect of vertical tidal flat accretion, lateral shoreline expansion and changing mean sea levels. As the vertical tidal flat accretion is relatively small over the 100 years (see Fig. 5), the differences between the two calculations thus predominantly reflect the impact of lateral expansion under SLR.

In the fixed tidal frame, the intertidal flat areas in the tidal basin largely decrease over time in the reference scenario, as a result of continued sediment loss to the sea. For the SLR scenarios, the reduction in intertidal area is slightly smaller compared with the reference case (Fig. 7a), as indicated by the vertical flat accretion under SLR (see Fig. 5). It suggests that the intertidal flats inside the tidal basin are less eroded under SLR, which is confirmed by a smaller surface area at low water (Fig. 8a). However, more sediment export occurs in the SLR scenarios, which is partly ascribed to the enlarged tidal prism (see Fig. S9). In contrast, the ebb-tidal delta exhibits an increase in intertidal area in the reference scenario due to a net sediment gain, and SLR leads to more accretion over the tidal flats as expected (Fig. 7c).

Considering a moving tidal frame, the reduction in intertidal flat areas becomes much smaller within the tidal basin, while a shift to increase occurs in the scenarios considering SLR >5 mm yr^{-1} (Figs. 7b and S10). The increase in intertidal flat areas is much more profound under a SLR of 1.0 and 2.0 m. The increase in intertidal area inside the tidal basin is predominantly ascribed to the newly-inundated floodplains that are converted from supra-into inter-tidal flats. This is also confirmed by a larger increase in surface area at high water than low water (Fig. 8b).

Similarly, the increase in intertidal flat area in the ebb-tidal delta becomes smaller under low SLR and a shift to a decrease occurs in the scenarios with SLR of 1.0 and 2.0 m (Fig. 7d). It suggests that the intertidal area in the ebb-tidal delta continues to increase under low SLR (albeit at a smaller rate compared with the reference scenario), but the intertidal area decreases in the high SLR scenarios. Overall, the vertical tidal flat accretion rates in the ebb-tidal delta lag behind higher SLR rates, despite more sediment supply from the tidal basin.

Detection of the changes in the low (low water to mean water) and high (mean water to high water) intertidal flats separately further demonstrates the influence of lateral expansion. When considering a moving tidal frame, the high intertidal flat areas are overall larger than the low flat areas inside the tidal basin, i.e., the former is approximately twice of the latter at the beginning, because of the concave flat profile shape (Fig. 8). The low intertidal areas increase by ~16% over the 100 years in the reference scenario, and the increase becomes more significant in the SLR scenarios (Fig. S11a). The high intertidal areas, however, decrease by ~15% in the reference scenario, and a low SLR slows down the decrease whereas a high SLR induces a rapid increase, particularly in the last 50 years (Fig. S11b). In contrast, low intertidal areas are larger than the high flat areas in the ebb-tidal delta region (Figs. S11c and S11d), suggesting the natural build-up of tidal flats; both the low and high flat areas increase over time in the reference scenario, while SLR induces a shift to decrease, particularly in the high intertidal areas. The decrease in high intertidal areas (Fig. S11d) dominates the reduction in the total intertidal areas (Fig. 7d) in response to SLR.

3.4. Volume changes

Both the channel volumes of the tidal basin below the mean water level and low water increase over time in all scenarios (Fig. 9a), which is consistent with the result of net sediment export (see Fig. 6). The intertidal storage volume does not show monotonic change, but a

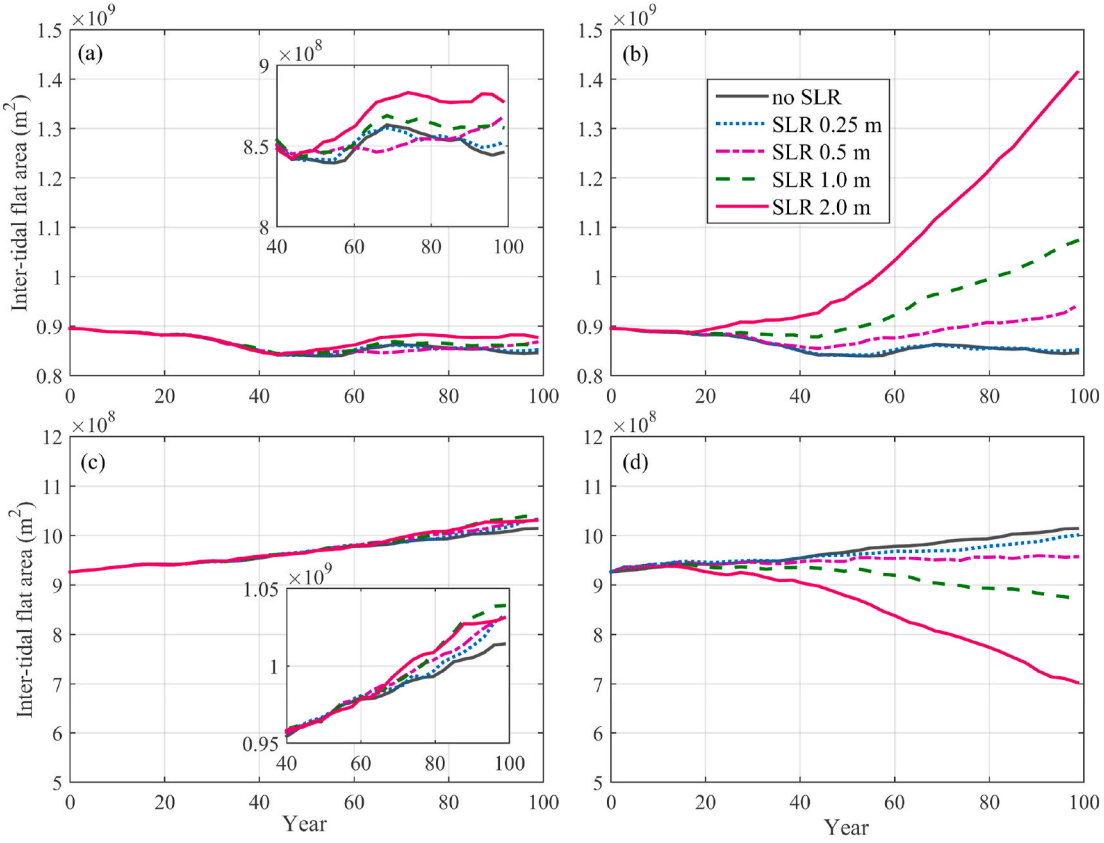

Fig. 7. Inter-tidal flat area changes in the tidal basin (a, b) and in the ebb-tidal delta (c, d) with respect to a fixed tidal frame (a, c) and with respect to a moving frame of reference level following SLR (b, d). The inset plots in (a) and (c) expand the last 60 years.

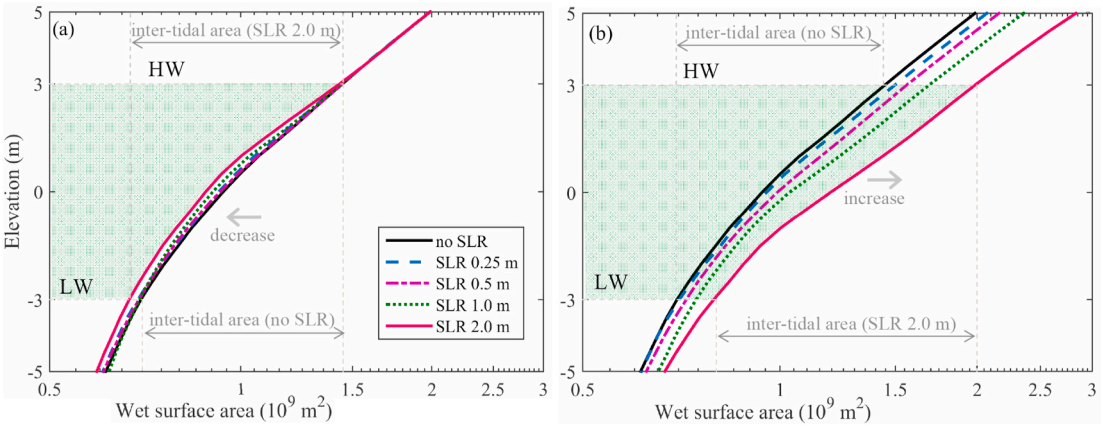

Fig. 8. Hypsometry changes (sub-tidal to supra-tidal zones) of the tidal basin in the (a) fixed frame of reference level, where the 0 datum of mean tide level is unchanged, and (b) a moving frame of reference level, where the 0 datum is adjusted to reflect the change in sea level after 100 years.

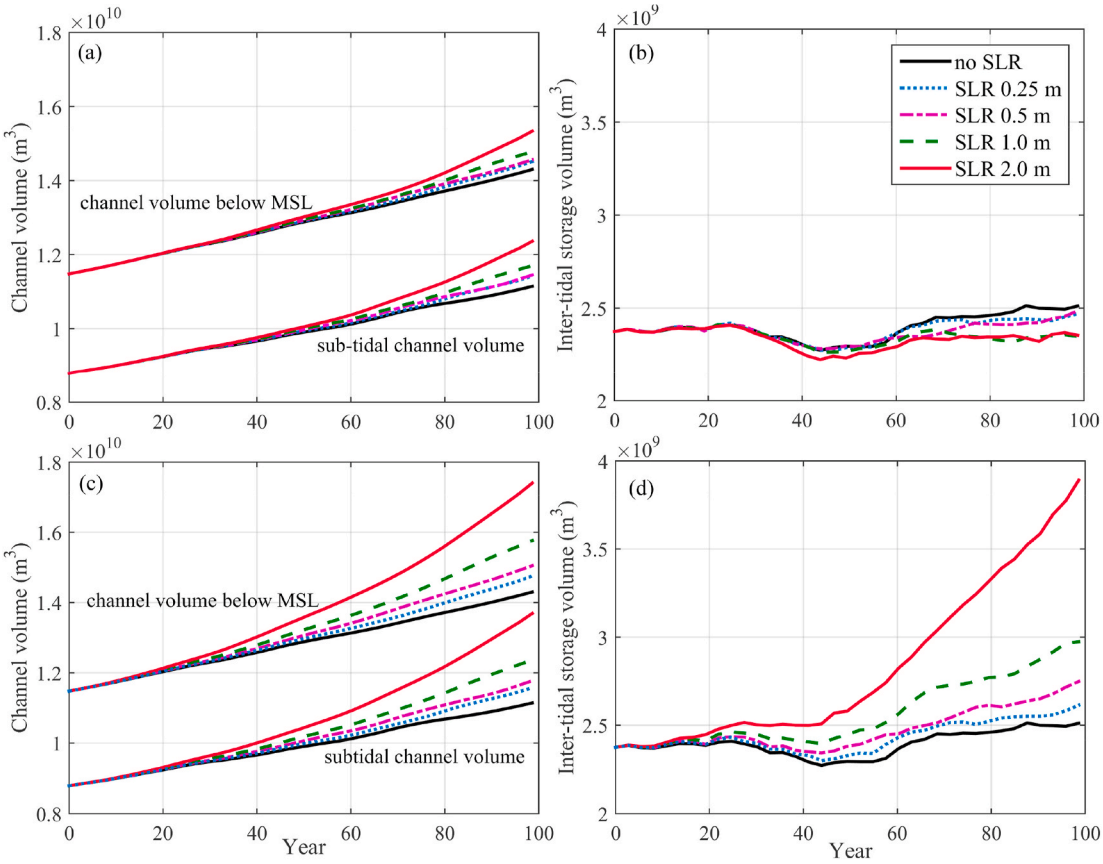

Fig. 9. Changes of (a, c) channel volumes below mean sea level (MSL) and low water (subtidal), and (b, d) intertidal storage volumes inside the tidal basin. The panels (a, b) and (c, d) are the results calculated according to fixed and moving tidal frames, respectively.

temporal decrease during the first 25–45 years, although the intertidal storage at the end of 100 years is larger than that at the beginning (Fig. 9b). SLR, however, induces a decrease in intertidal volume (evaluated on the fixed frame) compared with the reference scenario. Given that the intertidal area is comparatively larger in the SLR scenarios (see Fig. 7a), it suggests that the initially present intertidal zone gains sediment under SLR. Overall, these results indicate that SLR leads to subtidal channel erosion and intertidal accretion in the tidal basin.

The calculation on a moving tidal frame demonstrates that the increase in channel volumes is more significant under SLR (Fig. 9c). In contrast, the intertidal storage volume increases at a larger rate than the reference scenario (Fig. 9d). The differences in the calculation between the fixed and moving frames suggest the role of lateral expansion in modulating the channel-flat morphology as regards to the increase in plan areas, channel volumes, and inter-tidal storage volumes.

4. Discussion

4.1. Importance of lateral expansion

To indicate the importance of the low-lying land under SLR, we run extra simulations by removing the low-lying floodplains with elevation

above the high water at the beginning of the SLR scenarios, to represent a constrained tidal basin. The shorelines within the tidal basin are then fixed and do not migrate laterally under SLR (see Fig. S12). Compared with an unconstrained tidal basin (with low-lying lands), the tidal prism still increases with rising sea levels in the constrained basin, but at a smaller rate (see Fig. S9b). However, the sediment flux at the mouth does not increase with SLR compared with the reference scenario in the constrained basin (see Fig. 6b). The intertidal flat areas decrease at a larger rate compared with the reference scenario, which contrasts strongly with an increase in the unconstrained basin (see Fig. S13). It is because the constrained tidal basin exports sediment and the initially present tidal flats are submerged under SLR, both of which enhance the drowning of the tidal basin and the losses of intertidal flats.

The above comparison suggests that the low-lying land flanking the main channel is an important component of the dynamic behavior of the tidal basin by influencing tidal prism, tidal asymmetry and subsequent sediment transport. The hydraulic storage effect of intertidal zones is likely to induce stronger ebb currents, which leads to ebb dominance and sediment export (de Swart and Zimmerman, 2009; Robins and Davis, 2010; Ridderinkhof et al., 2014). The ebb dominance of net sediment transport in this study is attributed to the combined influence of the intertidal flat storage effect and a seaward return flow compensating the Stokes drift. The Stokes return flow becomes important in long tidal basins where non-standing waves develop (van der Wegen et al., 2008; Guo et al., 2014). The seaward residual current itself would induce seaward tidally-averaged sediment transport. Furthermore, its interaction with the oscillating tidal currents could drive seaward tidally-averaged sediment transport as well (Guo et al., 2014). Sediment export persists in all simulations, which is probably because static morphodynamic equilibrium has not been reached.

In addition, lateral shoreline migration and expansion under SLR creates new tidal flats, which compensate intertidal flat loss owing to drowning of the initially present flats. Moreover, the subsequent changes in basin geometry and hypsometry alter tidal asymmetry and associated sediment export. The SLR-induced change in tidal wave deformation is small as the amplitudes and phases of the principle tide and overtide change marginally. As the depth of the main channel increases under SLR, the magnitude of Stokes return flow would decrease, because it is distributed over a larger water column (Ridderinkhof et al., 2014). However, the intertidal storage volume increases at a larger rate than the increase in channel volume in the SLR scenarios, which leads to a smaller reduction in the intertidal storage volume to channel volume ratio compared with the reference case, even an increase in the SLR 2.0 m scenario (see Fig. S14). Such changes suggest enlarged intertidal storage effect under SLR, which would dominate over the other changes and eventually enhance the ebb dominance. Moreover, the tidal prism increases at a larger rate when lateral expansion is allowed, which also benefits larger sediment transport flux. Although more sediment is exported out of the tidal basin under SLR, lateral expansion to low-lying floodplains makes new tidal flats which counteract the drowning impact of SLR.

The above discussion implies that allowing lateral expansion changes the system's morphodynamic behavior. An unconstrained tidal basin has a buffer capacity which, to some degree, alleviates the drowning effect of SLR through sediment redistribution within the system, both vertically and horizontally (Fig. 10). The tidal basin provides a space for tidal evolution under SLR. The altered tidal asymmetry then plays a role in redistributing sediment and controlling the direction of morphodynamic adaptation. Other than the consequence of a direct tidal flat loss under SLR, the morphodynamic adaptation of unconstrained tidal basins to SLR has larger variability than the situation in open coasts and river deltas, given the dynamic changes in mean water depth, tidal wave propagation, basin hypsometry, sediment redistribution and the morphodynamic feedback mechanism.

4.2. Impact of SLR

The morphodynamic modeling results demonstrate some of the likely impact of SLR on the types of estuaries considered. An increase in channel width and the areas of shallow tidal flats under SLR might result in a decrease in tidal amplitude, as tidal amplitude is negatively proportional to channel width (Jeuken et al., 2003). An increase in channel depth implies a smaller friction, which would increase tidal current velocity and tidal prism. This change would amplify tidal range in shallow tidal basins and estuaries (van der Wegen and Roelvink, 2008; van der Wegen et al., 2008). In this study, however, the water depth along the tidal basin is comparably large (>15 m), so that the tidal amplification is less sensitive to SLR because the fractional change in

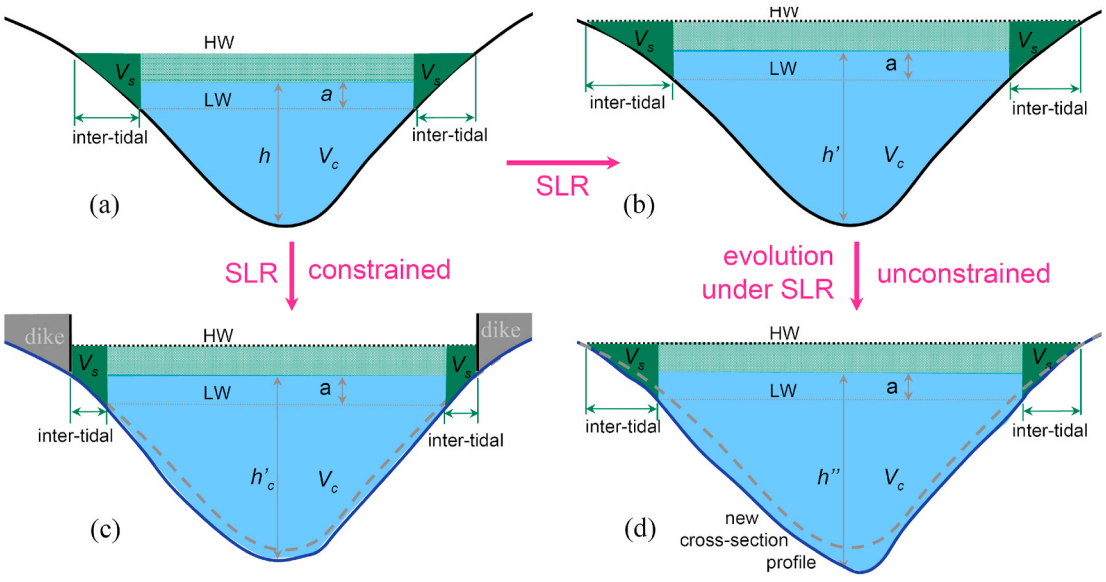

Fig. 10. Sketches showing the cross-section profile changes under SLR and consequent morphological evolution: (a) initial condition; (b) under SLR, and with morphological changes under SLR in (c) constrained and (d) unconstrained tidal basin. HW and LW indicate high water and low water, respectively, and V_c and V_s are channel volume below mean sea level and inter-tidal storage volume, respectively. The dashed lines indicate the new profiles considering morphodynamic adjustment under SLR.

both resonant frequency and frictional effect is buffered by the large depth (Talke and Jay, 2020).

When considering morphodynamic adaptations, SLR causes hypsometry changes by increasing water depth and inducing lateral expansion. The low relief of coastal plain tidal basins and the concave tidal flat profile imply the presence of a larger portion of high tidal flats than low tidal flats. Therefore, a small increase in mean sea level is likely to induce a large change in intertidal areas. The newly inundated low-lying lands under SLR have the potential to erode, which reduces their elevation. Moreover, the initial intertidal flats accrete under SLR but their vertical accretion rate lags behind SLR. For instance, the vertical accretion rate of the tidal flats in the tidal basin is approximately 2.2 mm yr^{-1} larger in the 1.0 m SLR scenario, compared with the reference case, which is smaller than the rate of SLR of 10 mm yr^{-1} (see Fig. S15). Hence, although SLR induces more sediment export, the intertidal flat zone inside the tidal basin laterally migrates and the intertidal area does not necessarily shrink.

The morphodynamic response of the ebb-tidal delta to SLR is similar to that of river-dominated deltas in past studies (van de Lageweg and Slangen, 2017). The exported sediments mainly deposit in the ebb-tidal delta front regions, which leads to more delta progradation (horizontal expansion in delta area) than aggradation (vertical increase in elevation) (Fig. S7). This is partially because the ebb-tidal delta keeps advancing given no waves and alongshore currents that transport the sediment away. The tidal flats over the ebb-tidal delta are drowned under SLR although more sediment is available. When taking the tidal basin and ebb-tidal delta as a whole into consideration, their total intertidal areas do not decrease owing to the lateral expansion under SLR.

The vertical flat accretion rate does not match SLR at the centennial time scale. The impact of SLR is much more significant in the last 50 years owing to a prescribed exponential increase in sea level over time. From this study and previous studies (van der Wegen, 2013), one explanation is that the morphodynamic adaptation occurs at a slower rate than the changes in sea level and associated hydrodynamics. The adaptation time scale of large-scale morphodynamics is very large, possibly longer than 100 years (van der Wegen, 2013; Lodder et al., 2019). Note that the morphodynamic time scale of a tidal basin is dependent on system dynamics like tidal strength, accommodation space, and the amounts of sediment being transported during a tidal cycle. Previous studies reported that the morphodynamic time scale is comparably shorter for the Humber Estuary in the UK (e.g., ~40 years) and longer for the Western Scheldt Estuary in the Netherlands (e.g., >100 years) (Jeuken et al., 2003). This time scale difference could influence the morphodynamic behavior in response to long-term changes like nodal tide and sea level (Wang and Townend, 2012). Determination of the morphodynamic time scale of simplified systems can be made by considering basin surface area, channel volume, and sediment concentrations etc. (Kragtwijk et al., 2004; Townend et al., 2016), but it remains technically challenging for complicated systems. Another uncertainty is that the morphodynamic time-scale in the model may not match that of estuaries in nature, due to the use of the morphological acceleration approach and the simplified settings.

4.3. Limitations and implications of this study

Interpretation of the findings from the schematized tidal basin should be confined to the forcing and boundary conditions in this study. The tides are very much amplified inside the tidal basin owing to strong channel convergence, with tidal ranges >4.0 m, which represents a macro-tidal environment (Davis, 1964). The strong tides stimulate morphodynamic development and rapid formation of the channel-shoal structure in the initial 500 years. In addition, a large tidal range is accompanied by a wide intertidal zone, which serves to highlight the potential impact of SLR on more inundation of low-lying lands. Lateral expansion would be at a smaller rate in meso- or micro-tidal environments, and sediment transport and morphodynamic adjustment rate might be also smaller and slower. Therefore, micro-tidal systems are likely to be more vulnerable to SLR compared with macro-tidal systems. Moreover, including overtides at the seaward boundary of the modeled estuary would induce additional tidal asymmetry and modulate the direction and magnitude of residual sediment transport. For instance, including overtides may induce landward residual sediment transport (sediment import), which counteracts the impact of Stokes flow in inducing seaward residual transport (Guo et al., 2014). Tidal asymmetry caused by overtides is largely response for the sediment import in the real systems like the Humber Estuary and the Dutch Wadden Sea (Townend and Whitehead, 2003; Wang et al., 2018).

River flow and associated sediment supply are excluded in this modeling study, making the schematized system more like a tidal embayment than an estuary. An extra simulation considering a river discharge of 1000 m^3/s in the same schematized basin exhibits a similar channel-shoal pattern to the tidally-dominated case (not shown). Including a larger river flow would induce a number of more complex dynamic processes, including raised subtidal water levels, enhanced subtidal currents and associated seaward sediment flushing capacity, water stratification and density currents (Guo et al., 2014; Olabarrieta et al., 2018; Zhou et al., 2020). Guo et al. (2014) suggested that even a small river discharge could overrule the role of tides in controlling tidally-averaged sediment transport and reinforce the seaward sediment flushing and inducing basin emptying, while a high river discharge induces more sediment supply and dampens the tide, which is likely to cause basin infilling. As the sediment export is enhanced by river flow, it becomes more difficult to sort out the control and the impact of basin hypsometry change on sediment flux. Sediment availability is also important for estuarine morphodynamic adaptation. For instance, external sediment sources from river and/or coasts may alter the balance of sediment import/export in tidal basins, e.g., increasing the sediment distribution within the tidal estuary and the resilience to SLR. Another factor not considered in this study was the impact of SLR in the presence of waves and storms. Waves and associated alongshore currents would remove sediment from the ebb-tidal delta and transport them away, which tends to reduce delta progradation. This may explain the continuous delta progradation in this modeling study. As the mean sea-level rises and the water depth becomes larger, the wave impacts may reach more inland and may alter the tidal flat morphology particularly over the ebb-tidal delta front region. Further investigation of the influence of SLR in estuaries considering river flow and riverine sediment supply and wave forcing would provide greater insight.

The initial morphology and simplified setting in this study might also influence the findings about the impact of SLR. The physical length of a tidal basin has impact on tidal wave propagation and subsequent morphodynamics, therefore tidal basins of varying lengths and geometry respond to SLR differently (Du et al., 2018). Morphodynamic adaptation to SLR in short tidal basins and lagoons (basin length « tidal wave length) can be different from the long tidal basin in this study, given that standing waves and synchronous tides are prone to occur in short basins. For instance, Dissanayake et al. (2012) found enhanced flood dominance and sediment import in a short tidal inlet-basin system under SLR of 2–7 mm yr^{-1} over 110 years, whereas van Maanen et al. (2013) reported enhanced sediment export in a similar but smaller system under SLR of 2.8–11.2 mm yr^{-1} over 200 years. The contrasting results are attributed to the size and shape of the tidal basins which affect tidal evolution and tidal asymmetry under SLR. The shape and gradient of the tidal flat profiles affect the system's buffering capacity to SLR. The concave profile shape in this study benefits submergence of low-lying land under SLR. The morphodynamic adaptation of tidal basin to SLR under different cross-section geometry requires site-specific investigation (Friedrichs et al., 1990; Leuven et al., 2019).

The net sediment export reproduced in this study may be overestimated because mud transport is excluded. Consideration of both sand and mud transports may induce more complex behavior given different mechanisms in controlling tidally-averaged transport of coarse

and fine sediments (Dronkers, 1986). For example, the export of sand and import of mud leading to net sediment import are detected in actual estuaries such as the Western Scheldt Estuary (Dam et al., 2007) and the Humber Estuary (Townend and Whitehead, 2003). SLR in such systems leads to an increase in accommodation space, which implies that more sediment import is needed as the system seeks to restore equilibrium (Townend et al., 2007; van der Wegen, 2013; Lodder et al., 2019). Although the model size and forcing conditions in the schematized model were prescribed to be similar to that of the North Branch in the Changjiang Estuary (Guo et al., 2021), the modeled channel pattern is more braided and bifurcated compared with the two-channel configuration found in reality. This difference is probably because mud transport, waves and alongshore currents acting on the North Branch were all excluded. Making the distinction between suspended and bedload transport of sand (e.g., using other sediment transport formula) and including mud transport might change the sediment export regime and the channel pattern over the ebb-tidal delta region depending upon the relative contents of mud and sand, which needs future in-depth study (Hepkema et al., 2019; Lenstra et al., 2019).

The initial morphology used in the SLR scenario simulations might have not approached an equilibrium state yet, although the morphological change rate has slowed down. In an ideal case it would be better to model and analyze the SLR impact when a morphodynamic equilibrium is reached, but morphodynamic equilibrium, either a static or dynamic equilibrium, is technically hard to define (Zhou et al., 2017) and may require much longer computation time for such a large-scale system. van der Wegen (2013) has examined morphodynamic evolution with SLR under different initial bathymetries and found that the overall change in behavior persists, although the change rates are slightly different. This suggests that the interpretation of SLR impact is not unduly influenced by the initial morphology in the model. It may also be because the impact of the initial morphology is no longer morphologically significant, when compared with the sea level perturbation imposed.

The model-produced morphology may also be sensitive to other physical settings like the dry cell erosion parameter and the bed slope effect. Extra sensitivity simulations to examine the role of the dry cell erosion parameter suggests slightly smaller lateral shoreline migration rates when the dry cell erosion function is not activated (0%), or with a smaller dry cell erosion parameter of 50%, compared with the results of 100% (see Fig. S16). However, the impact on the channel-shoal pattern and the cumulated sediment flux at the mouth section is overall less apparent. It is worth noting that the dry bed erosion function only produces gradual erosion of the dry cells and does not capture other lateral processes like bank collapse and cliff formation. The latter needs extra physical processes such as those examined by Zhao et al. (2019). Extra sensitivity simulations considering smaller (alfaBn = 5) and larger (alfaBn = 20) lateral bed slope effect reveals a more significant impact on the morphology. A smaller lateral bed slope effect leads to more braided channel pattern and larger transverse bed slope between the channels and shoals, while a larger lateral bed slope effect flattens the morphology and leads to less tidal flat area (see Fig. S17). These sensitivity model results are consistent with the results in Dissanayake et al. (2012) and Baar et al. (2019), demonstrating the necessity to choose a suitable representation of the bed slope effect when modeling long-term and larger-scale alluvial morphodynamics.

This study examines the physical processes only, while the potential impact of vegetation on tidal flat accretion is not considered. The vegetated tidal flats tend to have a larger erosion resistance owing to the root-enhanced substrate contexts, which is likely to reduce dry land erosion. In addition, vegetation stimulates salt-marsh accretion compared with bare flats by increasing sediment trapping in the vegetated regions. Moreover, accumulation of underground organic matter in salt-marshes may also help tidal flat accretion (Thorne et al., 2018). There is increasing evidence that considering the ecological impact of the vegetation canopy can increase the resilience of tidal flats and salt-marshes to SLR (Kirwan et al., 2016; Best et al., 2018). The vegetation canopy is also expected to migrate landward to low-lying land in response to SLR if there is space (Enwright et al., 2016). For example, coastal salt-marsh and mangrove migration under SLR has been detected over Holocene and modern time scales (Cohen et al., 2020). Examination of the mutual evolution of the vegetation and morphology is an emerging topic (Murray et al., 2008; Pelling et al., 2013) and merits future study.

Although the schematized model is not supposed to represent specific tidal basins or estuaries in nature, the model domain and forcing settings mimic tide-dominated long tidal basins in coastal plains with low relief which can shed light on their morphodynamic behavior in response to SLR. The model results suggest that the tidal flats in the coupled tidal basin and ebb-tidal delta system might survive a low SLR over 100 years, while the drowning impact of a high SLR is mitigated by a negative feedback between geometric change, tidal evolution and morphodynamic adjustment, when lateral expansion is possible. It thus highlights the importance of conserving floodplains and wetlands surrounding tidal channels that provide a critical buffering capacity. However, human activities such as tidal flat reclamation, channel dredging, and construction of dikes and jetties to realign navigation channels (Boltt et al., 2006; Zhao et al., 2018) have substantially modified estuarine morphodynamics and constrained the free behavior of tidal basins and estuaries in the past centuries, such as in the Western Scheldt Estuary (Dam et al., 2013; see Fig. S1a) and in the North Branch of the Changjiang Estuary (Guo et al., 2021). Constraining tidal systems by constructing extensive dikes and reclaiming low-lying floodplains, wetlands, and intertidal flats may significantly affect tidal propagation and amplification (Pelling et al., 2013; Talke and Jay, 2020) and reduce the systems' resilience to SLR. This confirms the ongoing mindset change in coastal defense and management reflected in the increasing popularity of soft engineering schemes which leave or restore space for nature (Temmerman et al., 2013; Bouma et al., 2014).

5. Conclusions

Understanding the impact of SLR on tidal basins and estuaries in the coming 100 years is of practical interest for coastal management and human development. In this work we deployed a numerical model to explore centennial morphodynamic evolution of a schematized tidal basin with broad tidal flats in response to SLR up to a rate of 20 mm yr^{-1}. We find that sediment export at the basin mouth increased with SLR, owing to increased hydraulic storage on the tidal flats, which favors ebb dominance. The intertidal flat areas throughout the tidal basin and ebb-tidal delta increase under a low SLR, e.g., 2.5 mm yr^{-1} in this study. The intertidal flat areas still increase in the tidal basin under a higher SLR owing to lateral incursion, which converts sub-aerial floodplains into intertidal flats, while the ebb-tidal delta loses intertidal flats although it receives more sediment. The latter is because the vertical flat accretion occurs at a rate smaller than SLR, which is in turn partly because morphodynamic evolution is in essence much slower compared with the changes in mean sea level and tidal hydrodynamic adaptation.

The model results suggest that an unconstrained tidal basin can adapt to low SLR and has some resilience to high SLR by creating new flats and redistributing sediment. Further work is needed to consider river flow and associated sediment supply, initial presence of overtides at the seaward boundary, waves, suspended transport of sand and cohesive sediment, and interaction between biological and morphological evolution to better understand the tidal basin morphodynamic variability and its adaptation to SLR. These forcing and processes may lead to more variability in the direction and magnitude of the residual sediment transport and alter the morphodynamic adaptation time scale. Including external sediment source from river and coasts would increase the sediment availability in the estuary and possibly the resilience to SLR. Although interpretation of the model results can be influenced by the simplified model settings, the findings in this work provide insights

into how SLR may affect natural tidal basin with a strong morphodynamic feedback. It clearly demonstrates the importance of conserving low-lying floodplains and wetlands surrounding tidal channels, which could sustain tidal basin systems' buffering capacity in response to SLR.

Declaration of competing interest

The authors declare that they have no known competing financial interests or personal relationships that could have appeared to influence the work reported in this paper.

Acknowledgements

This work is supported by the Ministry of Science and Technology, P. R. China (MOST) (No. 2017YFE0107400; 2016YFE0133700), Natural Science Foundation of China (Nos. 51739005; U2040216; 41876091), and the Science and Technology Commission of Shanghai Municipality (Nos. 19QA1402900; 20DZ1204700).

Appendix A. Supplementary data

Supplementary data to this article can be found online at https://doi.org/10.1016/j.csr.2021.104494.

References

Allen, J.R.L., 1990. The Severn Estuary of southwest Britain: its retreat under marine transgression, and fine sediment regime. Sediment. Geol. 66 (1–2), 13–28.

Bagnold, R.A., 1966. An approach to the sediment transport problem from general physics. US Geological Survey Prof paper 422-I, Washington, USA.

Bamunawala, J., Dastheib, A., Ranasinghe, R., van der Spek, A., Maskey, S., Murray, A.B., Duong, T.M., Barnard, P.L., Sirisena, T.A.J.G., 2020. A holistic modeling approach to project the evolution of inlet-interrupted coastlines over the 21st century. Frontiers in Marine Science 7. https://doi.org/10.3389/fmars.2020.00542.

Baar, A.W., Albernaz, M.B., van Dijk, W.M., Kleinhans, M.G., 2019. Critical dependence of morphodynamic models of fluvial and tidal systems on empirical downslope sediment transport. Nat. Commun. 10 (1), 1–12.

Best, U.S.N., van der Wegen, M., Dirkstra, J., Willemsen, P.W.J.M., Borsje, B.W., Roelvink, D.J.A., 2018. Do salt marshes survive sea level rise? Modeling wave action, morphodynamics and vegetation dynamics. Environ. Model. Software 109, 152–166.

Blum, M.D., Roberts, H.H., 2009. Drowning of the Mississippi Delta due to insufficient sediment supply and global sea-level rise. Nature. https://doi.org/10.1038/NGE0553.

Bouma, T.J., van Belzen, J., Balke, T., Zhu, Z.C., Airoldi, L., Blight, A.J., Davis, A.J., Galvan, C., Hawkins, S.J., Hoggart, S.P.G., Lara, J.L., Losada, I.J., Maze, M., Ondiviela, B., Skow, M.W., Strain, E.M., Thompson, R.C., Yang, S.L., Zanuttigh, B., Zhang, L.Q., Herman, P.M.J., 2014. Identifying knowledge gaps hampering application of intertidal habitats in coastal protection: opportunities & steps to take. Coast. Eng. 87, 147–157.

Chen, X.Y., Zhang, X.B., Church, J.A., Watson, C.S., King, M.A., Monselesan, D., Legresy, B., Harig, C., 2017. The increasing rate of global mean sea-level rise during 1993-2014. Nat. Clim. Change. https://doi.org/10.1038/NCLIMATE3325.

Church, J.A., Clark, P.U., Cazenave, A., Gregory, J.M., Jevrejeva, S., Levermann, A., Merrifield, M.A., Milne, G.A., Nerem, R.S., Nunn, P.D., Payne, A.J., Pfeffer, W.T., Stammer, D., Unnikrishnan, A.S., 2013. sea level change. In: Stocker, T.F., Qin, D., Plattner, G.-K., Tignor, M., Allen, S.K., Boschung, J., Nauels, A., Xia, Y., Bex, V., Midgley, P.M. (Eds.), Climate Change 2013: the Physical Science Basis. Contribution of Working Group I to the Fifth Assessment Report of the Intergovernmental Panel on Climate Change. Cambridge University Press, Cambridge, United Kingdom and New York, NY, USA.

Cohen, M.C.L., Figueiredo, B.L., Oliveira, N.N., Fontes, N.A., Franca, M.C., Pessenda, L.C. R., de Souza, A.V., Macario, K., Giannini, P.C.F., Bendassoli, J.A., Lima, P., 2020. Impact of Holocene and modern sea-level changes on estuarine mangroves from northeastern Brazil. Earth Surf. Process. Landforms. https://doi.org/10.1002/esp.4737.

Craft, C.B., Clough, J., Ehman, J., Joye, S.B., Park, R., Pennings, S.C., Guo, H., Machmuller, M., 2009. Forecasting the effects of accelerated sea level rise on tidal marsh ecosystem services. Front. Ecol. Environ. 7, 73–78.

Dalrymple, R.W., Leckie, D.A., Tillman, R.W., 2006. Incised Valleys in Time and Space. Society for Sedimentary Geology 2006, Tulsa, Okla.

Dalrymple, R.W., Choi, K.S., 2007. Morphologic and facies trends through the fluvial-marine transition in tide-dominated depositional systems: a systematic framework for environmental and sequence-stratigraphic interpretation. Earth Sci. Rev. 81, 135–174.

Dam, G., Bliek, A.J., Labeur, R.J., Ides, S.J., Plancke, Y.M.G., 2007. Long-term process-based morphological model of the western Scheldt estuary. In: Dohmen-Janssen, C. M., Hulscher, J.M.H. (Eds.), Proceedings of the 5th IAHR Symposium on River, Coastal and Estuarine Morphodynamics. https://doi.org/10.1201/NOE0415453639-c135.

Dam, G., van der Wegen, M., Roelvink, D., 2013. Long-term performance of process-based models in estuaries. Proceedings of the Coastal Dynamics Conference 409–419.

Dangendorf, S., Marcos, M., Woppelmann, G., Conrad, C.P., Frederikse, T., Riva, R., 2017. Reassessment of 20th century global mean sea level rise. Proc. Natl. Acad. Sci. Unit. States Am. 114, 5964-5951.

Davis, J.L., 1964. A morphogenic approach to world shorelines. Zeitschrift fur Geomorphologie 8, 127–142.

de Swart, H.E., Zimmerman, J.T.F., 2009. Morphodynamics of tidal inlet systems. Annu. Rev. Fluid Mech. 41, 203–229.

Deltares, 2011. User Manual Delft3D-Flow: Simulation of Multi-Dimensional Hydrodynamic Flows and Transport Phenomena, Including Sediments. Deltares, Delft, Netherlands. Version 3.15.

Dissanayake, D.M.P.K., Ranasinghe, R., Roelvink, J.A., 2012. The morphological response of large tidal inlet/basin systems to relative sea level rise. Climate Change 113 (2), 253–276. https://doi.org/10.1007/s10584-012-0402-z.

Douglas, B.C., 1991. Global sea level rise. J. Geophys. Res. 96 (C4), 6981–6992.

Dronkers, J., 1986. Tidal asymmetry and estuarine morphology. Neth. J. Sea Res. 20 (2/3), 117–131.

Du, J.B., Shen, J., Zhang, Y.L.J., Ye, F., Liu, Z., Wang, Z.G., Wang, Y.P., Yu, X., Sisson, M., Wang, H.V., 2018. Tidal responses to sea-level rise in different types of estuaries: the importance of length, bathymetry and geometry. Geophys. Res. Lett. 45, 227–235.

Elmilady, H., van der Wegen, M., Roelvink, D., Jaffe, B.E., 2019. Intertidal area disappears under sea level rise: 250 years of morphodynamic modeling in San Pablo Bay, California. J. Geophys. Res.: Earth Surface 124, 38–59.

Engelund, F., Hansen, E., 1967. A Monograph on Sediment Transport in Alluvial Streams. Teknisk-Forlag, Copenhagen.

Enwright, N.M., Griffith, K.T., Osland, M.J., 2016. Barrier to and opportunities for landward migration of coastal wetlands with sea-level rise. Front. Ecol. Environ.

Frederikse, T., Landerer, F., Caron, L., Adhikari, S., Parkes, D., Humphrey, V.W., Dangendorf, S., Hogarth, P., Zanna, L., Cheng, L.J., Wu, Y.H., 2020. The causes of sea-level rise since 1900. Nature 584, 393–397.

Friedrichs, C.T., 2011. Tidal flat morphodynamics: a synthesis. In: Flemming, B.W., Hansom, J.D. (Eds.), Treatise on Estuarine and Coastal Science, Estuarine and Coastal Geology and Geomorphology, vol. 3. Elsevier, Amsterdam, pp. 137–170.

Friedrichs, C.T., Aubrey, D.G., Speer, P.E., 1990. Impacts of relative sea-level rise on evolution of shallow estuaries. In: Cheng, R.T. (Ed.), Coastal and Estuarine Studies, vol. 38. Residual currents and long-term transport, Springer-Verlag, New York, US, pp. 105–120.

Ganju, N.K., Schoellhamer, D.H., 2010. Decadal-timescale estuarine geomorphic change under future scenarios of climate and sediment supply. Estuar. Coast 33, 15–29. https://doi.org/10.1007/s12237-009-9244-y.

Ganju, N.K., Defne, Z., Kirwan, M.L., Fagherazzi, S., D'Alpaos, A., Carniello, L., 2017. Spatially integrative metrics reveal hidden vulnerability of salt marshes. Nat. Commun. 8, 1–7. https://doi.org/10.1038/ncomms14156.

Guo, L.C., van der Wegen, M., Wang, Z.B., Roelvink, D., He, Q., 2015. Long-term, process-based morphodynamic modeling of a fluvio-deltaic system, Part I: the role of river discharge. Continent. Shelf Res. 109, 95–111.

Guo, L.C., Xie, W.M., Xu, F., Wang, X.Y., Zhu, C.Y., Meng, Y., Zhang, W.G., He, Q., 2021. A historical review of sediment export-import shift in the North Branch of Changjiang Estuary. Earth Surf. Process. Landforms. https://doi.org/10.1002/esp.5084.

Hepkema, T.M., de Swart, H.E., Schuttelaars, H.M., 2019. Sensitivity of tidal bar wavelength to channel width. J. Geophys. Res.: Earth Surface 124, 2417–2436.

Ikeda, S., 1982. Lateral bed load transport on side slopes. Journal Hydraulics Division, ASCE 108 (11), 1369–1373.

IPCC, 2014. Impacts, Adaptation, and Vulnerability. Part A: Global and Sectoral Aspects. Contribution of Working Group II to the Fifth Assessment Report of the Intergovernmental Panel on Climate Change. Cambridge University Press, Cambridge, United Kingdom and New York, NY, USA.

Jeuken, M.C.J.L., Wang, Z.B., Keiller, D., Townend, I., Liek, G.A., 2003. Morphological response of estuaries to nodal tide variations. In: Proceedings of the International Conference on Estuaries and Coasts, pp. 166–173. Hangzhou, China.

Kirby, R., 2000. Practical implications of tidal flat shape. Continent. Shelf Res. 20, 1061–1077.

Kirwan, M., Megonigal, J.P., 2013. Tidal wetland stability in the face of human impacts and sea-level rise. Nature 504, 53–60.

Kirwan, M., Temmerman, S., Keehan, E.E., Guntenspergen, G.R., Fagherazzi, S., 2016. Overestimation of marsh vulnerability sea level rise. Nat. Clim. Change 6 (3), 253–260.

Kragtwijk, N.G., Stive, M.J.F., Wang, Z.B., Zitman, T.J., 2004. Morphological response of tidal basins to human interventions. Coast. Eng. 51, 207–221.

Ladd, C.J.T., Duggan-Edwards, M.F., Bouma, T.J., Pages, J.F., Skov, M.W., 2019. Sediment supply explains long-term and large-scale patterns in saltmarsh lateral expansion and erosion. Geophys. Res. Lett. https://doi.org/10.1029/2019GL083315.

Lenstra, K.J.H., Ridderinkhof, W., van der Vegt, M., 2019. Unraveling the mechanisms that cause cyclic channel-shoal dynamics of ebb-tidal deltas: a numerical modeling study. J. Geophys. Res.: Earth Surface 124, 2778–2797.

Leuven, J.R.F.W., Pierik, H.J., van der Vegt, M., Bouma, T.J., Kleinhans, M.G., 2019. Sea-level-rise-induced threats depend on the size of tide-influenced estuaries worldwide. Nat. Clim. Change. https://doi.org/10.1038/s41558-019-0606-4.

Le Hir, P., Roberts, W., Cazaillet, O., Christie, M., Bassoullet, P., Bacher, C., 2000. Characterization of intertidal flat hydrodynamics. Continent. Shelf Res. 1433–1459.

Lesser, G.R., Roelvink, J.A., Van Kester, J.A.T.M., Stelling, G.S., 2004. Development and validation of a three-dimensional morphological model. Coast. Eng. 51, 883–915.
Lodder, Q.J., Wang, Z.B., Elias, E.P.L., van der Spek, A.J.F., de Looff, H., Townend, I.H., 2019. Future response of the Wadden Sea tidal basins to relative sea-level rise—an aggregated modelling approach. Water 11 (10). https://doi.org/10.3390/w11102198.
Mariotti, G., Carr, J., 2014. Dual role of salt marsh retreat: long-term loss and short-term resilience. Water Resour. Res. 50 (4), 2963–2974.
Muis, S., Verlaan, M., Winsemius, H.C., Aerts, J.C.J.H., Ward, P.J., 2016. A global reanalysis of storm surge and extreme sea levels. Nat. Commun. 7, 11969. https://doi.org/10.1038/ncomms11969.
Murray, A.B., Knaapen, M.A.F., Tal, M., Kirwan, M.L., 2008. Biomorphodynamics: physical-biological feedbacks that shape landscapes. Water Resour. Res. 44, W11301. https://doi.org/10.1029/2007WR006410.
Nerem, R.S., Chambers, D.P., Choe, C., Mitchum, G.T., 2010. Estimating mean sea level changes from the TOPEX and Jason altimeter missions. Mar. Geodes. 33, 435–446.
Nicholls, R.J., Hoozemans, F.M.J., Marchand, M., 1999. Increasing flood risk and wetland losses due to global sea-level-rise: regional and global analyses. Global Environ. Change 9, S69–S87.
Olabarrieta, M., Geyer, W.R., Coco, G., Friedrichs, C.T., Cao, Z., 2018. Effects of density-driven flows on the long-term morphodynamic evolution of funnel-shaped estuaries. J. Geophys. Res.: Earth Surface 123, 2901–2924.
Pelling, H.E., Green, J.A.M., Ward, S.L., 2013. Modelling tides and sea-level rise: to flood or not to flood. Ocean Model. 63, 21–29.
Ridderinkhof, W., de Swart, H.E., van der Vegt, M., Alebregtse, N.C., Hoekstra, P., 2014. Geometry of tidal inlet systems: a key factor for the net sediment transport in tidal inlets. J. Geophys. Res.: Oceans 119 (10), 6988–7006. https://doi.org/10.1002/2014jc010226.
Robins, P.E., Davis, A.G., 2010. Morphological controls in sandy estuaries: the influence of tidal flats and bathymetry on sediment transport. Ocean Dynam. 60, 503–517.
Roelvink, J.A., Walstra, D.J., 2004. Keeping it simple by using complex models. Advances in Hydro-science and Engineering 6, 1–11.
Roelvink, J.A., Reniers, A.J.H.M., 2011. A guide to coastal morphology modeling. In: Advances in Coastal and Ocean Engineering, vol. 12. World Sci. Co., Singapore.
Rossington, K., Nicholls, R.J., Knaapen, M.A.F., Wang, Z.B., 2007. Morphological behaviour of UK estuaries under conditions of accelerating sea level rise. In: Dohmen-Janssen, C.M., Hulscher, S.J.M.H. (Eds.), RCEM2007, River, Coastal and Estuarine Morphodynamics. Taylor & Francis.
Schuerch, M., Spencer, T., Temmerman, S., Kirwan, M., Wolff, C., Lincke, D., McOwen, C. J., Pickering, M.D., Reef, R., Vafeidis, A.T., Hinkel, J., Nicholls, R.J., Brown, S., 2018. Future response of global coastal wetlands to sea-level rise. Nature 561, 231–234.
Syvitski, J.P.M., Kettner, A., Overeem, I., Hutton, E.W.H., Hannon, M.T., Brakenridge, C. R., Day, J., Vorosmarty, C., Saito, Y., Giosan, L., Nicholls, R.J., 2009. Sinking deltas due to human activities. Nat. Geosci. 2, 681–686.
Takekawa, J.Y., Thorne, K.M., Buffington, K.J., Spragens, K.A., Swanson, K.M., Drexler, J.Z., Schoellhamer, D.H., Overton, C.T., Casazza, M.L., 2013. Final Report for Sea-Level Rise Response Modeling for San Francisco Bay Estuary Tidal Marshes. U.S. Geological Survey Open File. https://doi.org/10.3133/ofr20131081. Report 2013-1081.
Talke, S.A., Jay, D.A., 2020. Changing tides: the role of natural and anthropogenic factors. Annual Review of Marine Sciences 12, 14.1–14.31.
Temmerman, S., Meire, P., Bouma, T.J., Herman, P.M.J., Ysebaert, T., de Vriend, H.J., 2013. Ecosystem-based coastal defense in the face of global change. Nature 504, 79–83.
Thorne, K., MacDonald, G., Guntenspergen, G., Ambrose, R., Buffington, K., Dugger, B., Freeman, C., Janousek, C., Brown, L., Rosencranz, J., Holmquist, J., 2018. US Pacific coastal wetland resilience and vulnerability to sea-level rise. Science Advances 4 (2), eaao3270.
Townend, I.H., Pethick, J., 2002. Estuarine flooding and managed retreat. Phil. Trans. Roy. Soc. Lond. 360 (1796), 1477–1495.
Townend, I.H., Whitehead, P., 2003. A preliminary net sediment budget for the Humber Estuary. Sci. Total Environ. 314–316, 755–767.
Townend, I.H., Wang, Z.B., Rees, J.G., 2007. Millennial to annual volume changes in the Humber Estuary. Proceedings of the Royal Society A 463, 837–854.
Townend, I.H., Wang, Z.B., Stive, M., Zhou, Z., 2016. Development and extension of an aggregated scale model: part I- background to ASMITA. China Ocean Eng. 30 (4), 483–504.
Valiela, I., Lioret, J., Bowyer, T., Miner, S., Remsen, D., Elmstrom, E., Cogswell, C., Thieler, E.R., 2018. Transient coastal landscapes: rising sea level threatens salt marshes. Sci. Total Environ. 640–641, 1148–1156.
van de Lageweg, W.I., Slangen, A.B.A., 2017. Predicting dynamic coastal delta change in response to sea-level rise. J. Mar. Sci. Eng. 24, 1–12.
van Maanen, B., Coco, G., Bryan, K.R., Friedrichs, C.T., 2013. Modeling the morphodynamic response of tidal embayments to sea-level rise. Ocean Dynam. https://doi.org/10.1007/s10236-013-0649-6.
van der Wegen, M., Roelvink, J.A., 2008. Long-term morphodynamic evolution of a tidal embayment using a two-dimensional, process-based model. J. Geophys. Res. 113, C03016. https://doi.org/10.1029/2006JC003983.
van der Wegen, M., 2013. Numerical modeling of the impact of sea level rise on tidal basin morphodynamics. J. Geophys. Res.: Earth Surface 118, 447–460.
van der Wegen, M., Jaffe, B., Foxgrover, A., Roelvink, D., 2016. Mudflat morphodynamics and the impact of sea level rise in South San Francisco Bay. Estuar. Coast. https://doi.org/10.1007/s12237-016-0129-6.
van Goor, M.A., Zitman, T.J., Wang, Z.B., Stive, M.J.F., 2003. Impact of sea-level rise on the morphological equilibrium state of tidal inlets. Mar. Geol. 202, 211–227.
van Wijnen, H.J., Bakker, J.P., 2001. Long-term surface elevation change in salt marshes: a prediction of marsh response to future sea-level rise. Estuarine. Coastal and Shelf Science 52, 381–390.
Wang, Z.B., Townend, I.H., 2012. Influence of the nodal tide on the morphological response of estuaries. Mar. Geol. 291–294, 73–82.
Wang, Z.B., Elias, E.P.L., van der Spek, A.J.F., Lodder, Q.J., 2018. Sediment budget and morphological development of the Dutch Wadden Sea: impact of accelerated sea-level rise and subsidence until 2100. Neth. J. Geosci. 97, 183–214.
Wolanski, E., Chappell, J., 1996. The response of tropical Australian estuaries to a sea level rise. J. Mar. Syst. 7, 267–279.
Zhao, J., Guo, L.C., He, Q., Wang, Z.B., van Maren, D.S., Wang, X.Y., 2018. An analysis on half century morphological changes in the Changjiang Estuary: spatial variability under natural processes and human intervention. J. Mar. Syst. 181, 25–36.
Zhao, K., Gong, Z., Xu, F., Zhou, Z., 2019. The role of collapsed bank soil on tidal channel evolution: a process-based model involving bank collapse and sediment dynamics. Water Resour. Res. 55 https://doi.org/10.1029/2019WR025514.
Zhang, X.H., Leonardi, N., Donatelli, C., Fagherazzi, S., 2020. Divergence of sediment fluxes triggered by sea-level rise will reshape coastal bays. Geophys. Res. Lett. https://doi.org/10.1029/2020GL087862.
Zhou, Z., Coco, G., Townend, I., Olabarrieta, M., van der Wegen, M., Gong, Z., D'Alpaos, A., Gao, S., Jaffe, B.E., Gelfenbaum, G., He, Q., Wang, Y.P., Lanzoni, S., Wang, Z.B., Winterwerp, H., Zhang, C.K., 2017. Is 'morphodynamic equilibrium' and oxymoron? Earth Sci. Rev. 165, 257–267.
Zhou, Z., Chen, L.Y., Tao, J.F., Gong, Z., Guo, L.C., van der Wegen, M., Townend, I., Zhang, C.K., 2020. The role of salinity in fluvio-deltaic morphodynamics: a long-term modelling study. Earth Surf. Process. Landforms 45 (3), 590–604.